Role of the Fusion Peptide and Membrane-Proximal Domain in HIV-1 Envelope Glycoprotein-Mediated Membrane Fusion

Antony S. Dimitrov,[‡] Satinder S. Rawat,[‡] Shibo Jiang,[§] and Robert Blumenthal*,[‡]

Laboratory of Experimental and Computational Biology, Center for Cancer Research, National Cancer Institute, National Institutes of Health, Frederick, Maryland 21702, and Laboratory of Viral Immunology, Lindsley F. Kimball Research Institute, New York Blood Center, 310 East 67th Street, New York, New York 10021

Received July 3, 2003; Revised Manuscript Received October 3, 2003

ABSTRACT: The N-terminal fusion peptide and the interfacial sequence preceding the transmembrane anchor of HIV-1 gp41 are required for viral fusion. Studies with synthetic peptides indicated that these regions function by destabilizing membranes, which is regarded as a crucial step in the membrane fusion reaction. However, it is not clear whether membrane destabilization is induced by these sequences in the intact gp41. We address this question by examining fusion and destabilization of membranes expressing HIV-1_{IIIB} wild-type Env and two mutant Envs. (1) A Glu residue at position 2 of the gp41 fusion peptide is substituted for Val (V2E) to produce one mutant. (2) Residues 665−682 in the membrane-proximal domain are deleted to form the other. The process of membrane destabilization was monitored by the influx of Sytox, an impermeant fluorescent dye, into the Env-expressing cells following the interaction with CD4−CXCR4 complexes, and fusion was monitored by observing dye transfer between Env-expressing cells and appropriate target cells. We also monitored the conformational changes in the Envs following their interactions with CD4 and CXCR4 by immunofluorescence using an anti-gp41 mAb that reacts with the six-helix bundle. In contrast to the wild type, both Env mutants did not mediate cell fusion. The V2E Env did not mediate membrane destabilization. However, the Env with an unmodified fusion peptide but with a deletion of residues 665−682 in the membrane-proximal domain did mediate membrane destabilization. The wild type and both mutant Envs undergo conformational changes detected by the anti-gp41 six-helix bundle mAbs. Our results suggest that in intact HIV-1 Env the membrane-proximal domain is not required for membrane perturbations, but rather enables the bending of gp41 that is required for viral and target membranes to come together. Moreover, the observation that the Δ665−683 Env self-inserts its fusion peptide but does not cause fusion suggests that self-insertion of the fusion peptide is not sufficient for HIV-1 Env-mediated fusion.

Entry of HIV into a host cell requires the fusion of their membranes. Membrane fusion is driven by interaction of the HIV Env proteins, gp120 and gp41, with CD4 and a coreceptor, e.g., the chemokine receptor CXCR4 in our experiments (*1*−*4*). These interactions trigger a barrage of conformational changes that drive the membrane fusion process (*5*−*12*). According to the model of Chan and Kim, gp120 interacts with target cell CD4, and undergoes conformational changes leading to exposure of gp41, which forms a prehairpin intermediate (*8*). In this prehairpin intermediate, the fusion peptide of gp41, which is normally blocked by gp120, becomes exposed and inserts into the target membrane when such a target membrane is in the proximity. In a previous study, we showed that the membranes of the Env-expressing cells were compromised due to the interactions of Env with CD4 and cognate coreceptor attached to protein G beads (*7*). The transition of the gp41 prehairpin to a hairpin intermediate, in which the C-terminal helices form a six-helix bundle (6HB)[1] with the N-terminal heptad repeat peptide, is relatively slow, on the order of a couple of minutes, and is vulnerable to inhibition by C-peptides that mimic the sequence of the C-peptide repeat (*13*−*18*).

The role of the fusion peptide is crucial for the creation of perturbations in the cell membrane. However, other regions of gp41 may also be involved in the membrane destabilization and fusion. There are indications that a region from the gp41 ectodomain next to the transmembrane domain plays a significant role in the fusion process (*19*−*21*). However, it is not yet known whether this ectodomain

* To whom correspondence should be addressed: Center for Cancer Research, P.O. Box B, Bldg. 469, Rm. 216A, Miller Drive, Frederick, MD 21702-1201. Phone: (301) 846-1446. Fax: (301) 846-6192. E-mail: blumen@helix.nih.gov.

[‡] National Institutes of Health.

[§] New York Blood Center.

[1] Abbreviations: DMEM, Dulbecco's modified Eagle's cell culture medium; RPMI-1640, cell culture medium developed at Roswell Park Memorial Institute; D-PBS, Dulbecco's phosphate-buffered saline; V2E, mutant HIV-1 Env in which a Glu residue is substituted for Val at position 2 of the gp41 fusion peptide; Δ665−682, mutant HIV-1 Env in which residues 665−682 in the membrane-proximal domain are deleted; 6HB, six-helix bundle; CMTMR, 5(6)-{[(4-chloromethyl)-benzoyl]amino}tetramethylrhodamine; AraC, cytosine β-D-arabino-furanoside.

10.1021/bi035154g CCC: $25.00
Published on Web 11/13/2003

epitope influences the permeability of the Env-expressing membrane in the presence of CD4 and coreceptor. To examine whether the fusion peptide or the C-terminus of the gp41 ectodomain is responsible for destabilization of the membrane of the cells expressing Env, we performed mutational analysis. Freed and co-workers reported that a single mutation in the fusion peptide of HIV-1_{IIIB}, V2E, made gp41 nonfusogenic (*22*). Kliger and co-workers showed that a peptide that mimics the fusion peptide sequence induces liposome fusion, whereas the peptide with the V2E mutation does not (*23*). Another mutation in HIV-1_{IIIB} gp41 that involves the deletion of the region immediately next to the membrane-spanning domain (*19*) did not mediate HIV-1 fusion either. We used these two mutant Envs to examine the relationship between membrane destabilization and fusion.

In this study, we show that both Env mutants undergo conformational changes similar to those of the fusogenic wild-type Env using conformation specific monoclonal antibodies. We also show that deletion of the region of gp41 adjacent to the membrane-spanning domain preserves the ability to destabilize its own plasma membrane even though this mutant is unable to mediate fusion, whereas V2E was unable to induce fusion and membrane destabilization.

EXPERIMENTAL PROCEDURES

Plasmids. We used wild-type IIIB Env and the following Env mutants: V2E (Val in the second position of the fusion peptide replaced with Glu), Δ665−682 (deletion of residues 665−682 in the membrane-proximal region of gp41), and uncleaved, which has a mutation in the gp120−gp41 cleavage site. The V2E plasmid has a substitution at position 512, the hydrophilic glutamic acid replacing the hydrophobic valine (*22*−*24*). The Δ665−682 plasmid has a deleted KWASLWNWFSITNWLWYI sequence from the region immediately adjacent to the membrane-spanning domain (*19*, *20*). The uncleaved Env has a deletion of the gp120−gp41 cleavage site; i.e., the KRRVVQREKRAV sequence has been replaced by LR (*25*, *26*). The plasmids were kindly given to us by K. Salzwedel and E. A. Berger [National Institute of Allergy and Infectious Diseases (NIAID), National Institutes of Health]. We have amplified them by using the Qiagen (Valencia, CA) MaxiPrep kit.

Cells. We cultured HeLa cells in Dulbecco's modified Eagle's medium (DMEM) containing 10% fetal bovine serum (FBS) (DMEM-10), NIH3T3CD4X4 cells in DMEM-10 supplemented with 3 μg/mL Puromycin, SupT1 cells in RPMI medium 1640 supplemented with 10% FBS, and U373-MAGI-CXCR4 cells (NIH AIDS Research & Reference Reagent Program, catalog no. 3596) in DMEM containing 20% FBS, 300 μg/mL G418, and 200 μg/mL hygromycin B. All culture media contained 100 units/mL penicillin G and 100 μg/mL streptomycin sulfate.

Antibodies. To detect conformational changes, we used the mouse mAb, NC-1, which was designed against the six-helix bundle (6HB) of gp41 (*27*). To measure the level of Env expression, we used T8 (gift from C. Broder, F. Edward Hebert School of Medicine, Uniformed Services University of the Health Sciences, Bethesda, MD), which is a mouse anti gp120 mAb. As secondary antibodies we used goat anti-mouse IgG (H+L) polyclonal fragment antibodies (Fab) conjugated with Cy5 (Jackson Immunoresearch Laboratories, Inc., West Grove, PA). For the co-immunoprecipitation of CD4 and CXCR4, we used the anti-CXCR4 monoclonal mouse antibody 4G10 (gift from C. Broder, F. Edward Hebert School of Medicine, Uniformed Services University of the Health Sciences).

Transfections. Wild-type and mutant HIV-1 IIIB Env were expressed in HeLa cells by transfecting them with the respective *env* plasmids. Each plasmid was added at a final concentration of 0.02 mg/mL to a 0.06 mg/mL lipofectamine solution in DMEM-0 (without serum) in a glass tube and vortexed for 1 min, and then left to equilibrate for 1 h at room temperature. Aliquots (100 μL) of each plasmid suspension were added to HeLa cells previously plated in 12-well plates (2×10^5 cells per well). Incubation continued for 4 h at 37 °C with shaking every 10 min. In the last incubation hour, we added vaccinia vTF7.3 at a multiplicity of infection of 10. The addition of vTF7.3 or wild-type vaccinia is necessary at this point, because the *env* is under the control of the vaccinia promoter. At the end of the fourth hour, we added 1 mL of DMEM-10 per well and incubated the cells overnight at 31 °C to express the respective HIV-1 Env. To decrease the level of expression of the wild-type Env, we added AraC (cytosine β-D-arabinofuranoside, Sigma, St. Louis, MO) for the overnight incubation (*28*). The decreased level of expression of the wild-type Env allowed us to compare the membrane permeability induced by the Δ665−682 and wild-type Envs at the same expression levels.

CD4−CXCR4 Complexes on Protein G−Sepharose Beads. CD4−CXCR4 complexes were co-immunoprecipitated from U373CD4X4 cells as previously described (*7*, *29*). Briefly, the cells were washed with PBS, dissociated from the flask plate by using cell dissociation buffer, pelleted at 1500 rpm for 5 min, and resuspended at a final density of 10^7 cells/mL in lysis buffer, which contained 1% Brij97, 150 mM NaCl, 20 mM Tris (pH 8.2), 20 mM EDTA, protease inhibitors (1 μg/mL each of leupeptin, aprotinin, and pepstatin), and 5 mM iodoacetamide. Incubation continued for 2 h at 4 °C with gentle mixing. After cell lysis, the cell nuclei were pelleted by centrifugation at 17000*g* for 25 min in an Eppendorf centrifuge at 4 °C. Then, 1.5 μg of anti-CXCR4 antibody, 4G10, and a 15 μL suspension of protein G−Sepharose beads (Sigma) prewashed with PBS were added to each 1 mL supernatant. The suspensions were left for 14 h at 4 °C on a rotator so that the mAb, CXCR4, and associated CD4 would bind. Then they were washed four times with ice-cold lysis iodoacetamide-free buffer and once with ice-cold PBS and aliquoted.

HIV-Env-Mediated Fusion. The transfected HeLa cells were stained with CellTracker Orange CMTMR (5(6)-{[(4-chloromethyl)benzoyl]amino}tetramethylrhodamine) (Molecular Probes, Inc., Eugene, OR), washed, and covered with medium at 25 °C. Target cells, SupT1, preloaded with calcein AM (Molecular Probes, Inc.), were added, and the mixture was incubated at 25 °C for 25 min. Then the cells were washed once with medium to remove the unbound SupT1 and then covered with medium prewarmed at 37 °C. Incubation continued for 2 h at 37 °C with 5% CO_2. The level of fusion was determined as the ratio between Env-expressing cells that were stained with calcein and the total number of Env-expressing cells in contact with a target cell. We collected images of the cells and assessed fusion by using

MetaMorph 4.0 software (Universal Imaging Co., Downingtown, PA) (*5*).

HIV-Env Cell Membrane Permeability. Membrane permeability experiments were carried in a manner similar to that of the fusion experiments. The Env-expressing HeLa cells were stained with CellTracker Orange CMTMR, washed, and covered with medium at 25 °C. Bead−CD4−CXCR4 complexes were added and incubated at 25 °C for 25 min. Then the cells were washed once with medium and then covered with RPMI without serum prewarmed at 37 °C containing 0.5 μg/mL SYTOX Blue nucleic acid stain (Molecular Probes, Inc.). Incubation continued for 20 min at 37 °C with 5% CO_2. Membrane permeability was measured as the ratio of the cells stained by SYTOX Blue nucleic acid stain to the total number of cells, which were stained with CellTracker Orange CMTMR (*7*). We collected images and counted blue and red cells by using MetaMorph 4.0 software.

Immunofluorescence. To observe conformational changes in gp41, Env-expressing HeLa cells were incubated at 37 °C and CO_2 with bead−CD4−CXCR4 complexes for 5 min or with SupT1 cells for 10 min. After the incubation, the cells were immediately placed on ice to stop the fusion or permeabilization process. Cells were washed twice with ice-cold washing buffer (D-PBS with calcium and magnesium, Quality Biological, Inc., catalog no. 114-059-101, containing 0.1% bovine serum albumin and 0.02% sodium azide). Nonspecific Fab binding was blocked with blocking solution (2% normal goat serum in D-PBS) containing 1 μg/mL unconjugated Fab for 30 min on ice. Then, the cells were washed again twice with the washing buffer and once with 2% goat serum and incubated in 2% goat serum blocking solution supplemented with 1 μg/mL NC-1 mAb. Incubation continued for 1 h on ice. The cells were then washed twice with washing buffer and once with blocking solution and incubated with 1 μg/mL Cy5-conjugated goat anti-mouse Fab in blocking solution. Incubation with the secondary antibody continued for 1 h on ice. The cells were washed twice and covered with 1 mL of washing buffer per well prior to microscopic observation.

Env Expression. The Env expression was quantified by using the immunostaining procedure described above. After the transfections, the cells were cooled on ice. The Env was stained by using mouse anti-gp120 mAb, T8, as the primary antibody and Cy5-conjugated goat anti-mouse Fab as the secondary antibody. We collected images of the Cy5-stained cells and measured the fluorescence intensity of each image pixel. By using the built-in histogram function of the MetaMorph 4.0 software (Universal Imaging Co.), we collected the number of pixels that have the same positive fluorescence intensity and transferred the data into an MS Excel data sheet. The control for the intensity of nonspecific staining was determined by using HeLa cells infected with vaccinia vTF7.3 instead Env-expressing HeLa cells.

Microscopy. All images were collected by using a NIKON 200TE inverted microscope supplied with a PlanFluor 20×, ELWD, NA = 0.45 objective. We used single beam-splitter cubes: Nikon B-2E/C, 465−495/505/515−555 for the calcein staining, Nikon G-2E/C, 525−555/565/590−650 for the CellTracker Orange CMTMR, Cyan GFP V2, 426−446/455/460−500 (Chroma Technology Corp.) for the SYTOX Blue nucleic acid stain, and HQ41008, 590−650/660/663−738 (Chroma Technology Corp.) for the Cy5-conjugated Fab. The microscope was automated through the MetaMorph 4.0 software.

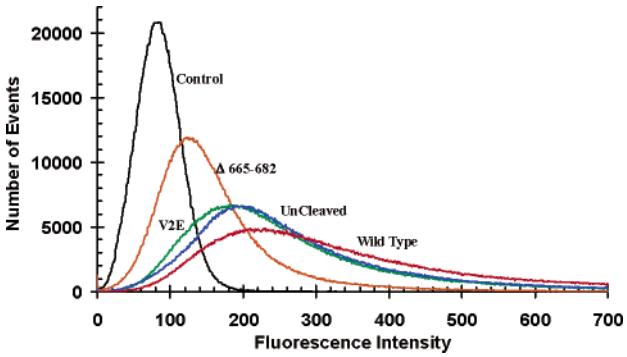

FIGURE 1: Expression of the IIIB mutant Envs on the HeLa cell surface. The Env gp120 was detected by using T8 mouse anti-gp120 mAb and Cy5-conjugated goat anti-mouse Fab. The images were digitized in 12 bit grayscale depth per pixel, corresponding to intensity levels from 0 to 4095. The median values of the fluorescence intensity for the wild-type, V2E, Δ665−682, and uncleaved Envs and control vTF7.3-infected cells were 220, 195, 175, 120, and 85, respectively.

RESULTS

Env Expression. Figure 1 shows the expression levels for the wild-type and mutant Envs on the cell membranes. The wild-type Env had the highest level of expression (with maximum counts at an intensity level of ∼220), and the mutant Env with amino acids 665−682 deleted had the lowest level of Env expression (with maximum counts at an intensity level of ∼120). The maximum counts for the nonspecific control staining of vTF7.3-infected HeLa cells appeared at an intensity level of 85. After 85 had been subtracted from the wild-type and Δ665−682 Env expression intensity levels, the wild-type Env exhibited a level of expression approximately 4 times higher than that of the Δ665−682 mutant (135 vs 35). Measurements of the surface concentrations of expressed Envs by immunofluorescence using the anti-gp120 antibody (T8) could be compromised by different exposures of gp120 epitopes in the mutant Envs, by the degree of Env proteolytic processing, or by potential gp120 shedding. However, Western blot analysis showed equal processing of wild-type (WT) and Δ665−682 Env (*19*) and of WT and V2E Env (*22*).

Fusion. Env-expressing HeLa cells were stained with CMTMR, and target SupT1 or NIH3T3CD4X4 cells were stained with calcein. During the fusion process, the calcein-stained cytoplasm of SupT1 or NIH3T3CD4X4 cells mixed with the cytoplasm of HeLa cells. Microscopy showed the merging of the green and red color for fused cells and separation for nonfused cells that are in close contact. The level of fusion of the wild-type Env with SupT1 was 33 ± 2%, which was the same as the level of fusion with NIH3T3CD4X4 cells. As expected, we did not observe any fusion with V2E and Δ665−682 mutants or with the uncleaved Env (see Figure 2) (*19*, *22*). Figure 2 shows a microscopic view in differential interference contrast and overlay of the HeLa Env-expressing cells (red) and SupT1 (green). The fused cells in Figure 2 (top right corner image) are colored in orange formed from the overlap of green and red.

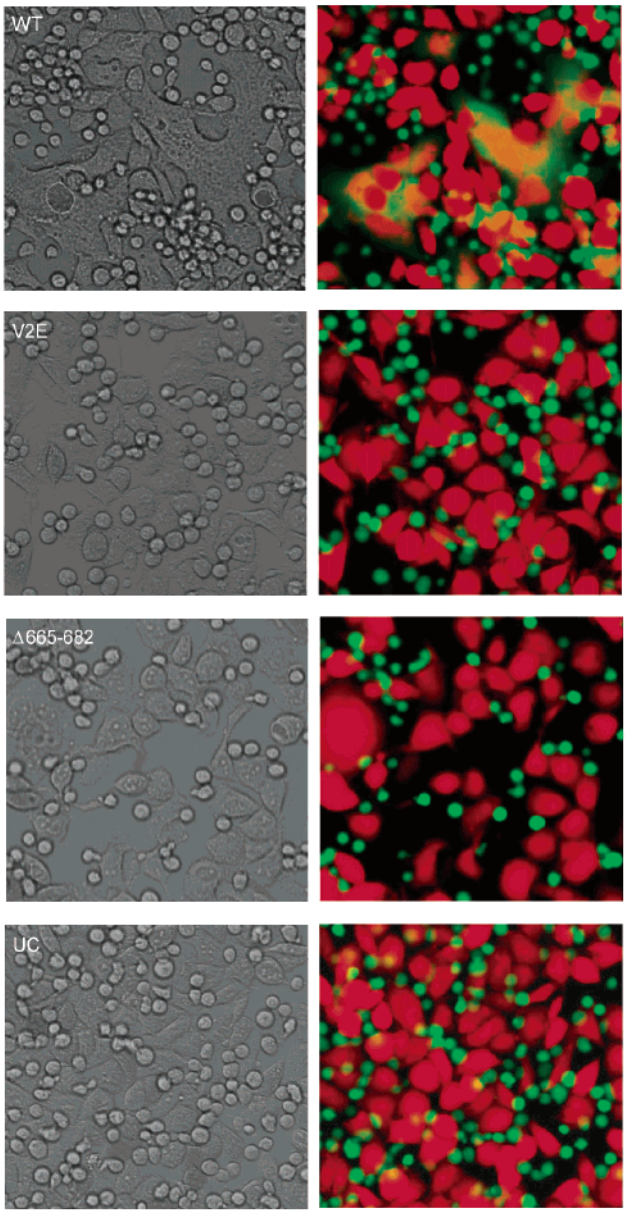

FIGURE 2: Fusion of Env-expressing HeLa cells with SupT1 after incubation for 2 h at 37 °C. HeLa cells were transfected with IIIB Env plasmids as follows: wild type in the first row, V2E mutant in the second row, Δ665−682 mutant in the third row, and uncleaved Env in the fourth row. The left column shows DIC images: HeLa cells plated and spread on the substrate while the SupT1 preserved their spherical shape if not fused. The right column shows an overlay of two fluorescence images. Env-expressing HeLa cells are red, and the SupT1 targets are green. Fusion of the SupT1 with the wild-type Env-expressing cells, seen like syncitia in DIC, appears orange as a result of the green and red merging.

Membrane Permeability. Figure 3A is a bar chart showing the percentage of cells with a compromised plasma membrane for the different Envs. The degree of membrane permeability (38 ± 2%) for the wild-type Env is similar to the degree of fusion for this Env (33 ± 3%). All our experiments showed a background of ∼5−8% of dead cells due to the vaccinia infection. Thus, the reading for the cell membrane permeability of the V2E Env-expressing cells (8.0 ± 1.5%) and uncleaved Env-expressing cells (5.5 ± 0.5%) was considered within the background. The membrane permeability of the Δ665−682 Env-expressing cells (19.0 ± 1.0%) was higher than the background, and we compared it to the membrane permeability of the wild-type Env-expressing cells. However, the Env expression level was higher for the wild-type Env. We were able to suppress the wild-type Env expression level by adding AraC to the medium. Figure 3B shows the Env expression level versus the concentration of AraC. Figure 3C shows the decrease in the membrane permeability for the wild-type Env-expressing cells versus AraC concentration. The median of the fluorescence intensity, which we defined here as a measure of the expression level, for the Δ665−682 Env was ∼120 (Figure 1), which coincided with the median fluorescence intensity level by the wild-type Env expressed in the presence of 320 nM AraC (Figure 3B). At this AraC concentration, the permeability of the wild-type Env-expressing membrane was 16.5 ± 3.5% (Figure 3C), which coincided well with the permeability of 19.0 ± 1.0% of the Δ665−682 Env-expressing membrane (Figure 3A). The median fluorescence intensity for V2E Env was ∼180 (Figure 1), which coincided well with the median fluorescence intensity for the wild-type Env expressed in the presence of 80 nM AraC (Figure 3B). At this AraC concentration, the permeability of the wild-type Env-expressing membrane was 30.5 ± 0.5% (Figure 3C), which obviously differed from the permeability of 8.0 ± 1.5% of the V2E Env-expressing membrane (Figure 3A). The median fluorescence intensity for the uncleaved Env was ∼200 (Figure 1), which corresponded to a fluorescence intensity level for the wild-type Env expressed in the presence of 60 nM AraC (interpolated plot in Figure 3B). At this AraC concentration, the permeability of the wild-type Env-expressing membrane should be ∼34.0% (interpolated curve in Figure 3C), which obviously differs from the permeability of 5.5 ± 0.5% of the uncleaved Env-expressing membrane (Figure 3A). Hence, the V2E and uncleaved Env-expressing membranes were not permeabilized by the CD4.X4 complexes, while the Δ665−682 Env-expressing membrane is permeabilized as well as the wild-type Env-expressing membrane (see Figure 3D).

Conformational changes of the Env precede membrane and cytoplasmic mixing in the fusion process (*5*). The lack of fusion or membrane permeability with V2E Env may be due to the lack of conformational changes. To test this, we examined the conformational changes in gp41 and gp120 in the presence of bead−CD4−CXCR4 complexes by using monoclonal antibodies against specific conformations. Usually, cell−cell binding leads to conformational changes in gp41 within the first 10 min (*30*). Because of the vast amount of receptors and coreceptors released from the bead−CD4−CXCR4 complexes, the conformational changes appeared faster, in the first 5 min when bead−CD4−CXCR4 complexes were used. Detection of the exposed gp41 epitope rapidly vanishes as the fusion or membrane permeabilization proceeds (data not shown). Figure 4A shows conformational changes in gp41 detected after incubation for 5 min with bead−CD4−CXCR4 complexes by using NC-1 mAb, which was specifically raised against six-helix bundle (6HB) formation (*27*). 6HB formation occurred in Env-expressing cells for the wild-type and mutant HIV-1 Envs. They were triggered by the receptors and coreceptors released by the beads. Occurrences of the 6HBs were detected by immunostaining with NC-1 and Cy5-conjugated anti-mouse Fab. The fluorescence images taken after immunostaining were digitally enhanced to contrast the 6HB occurrence on the cell

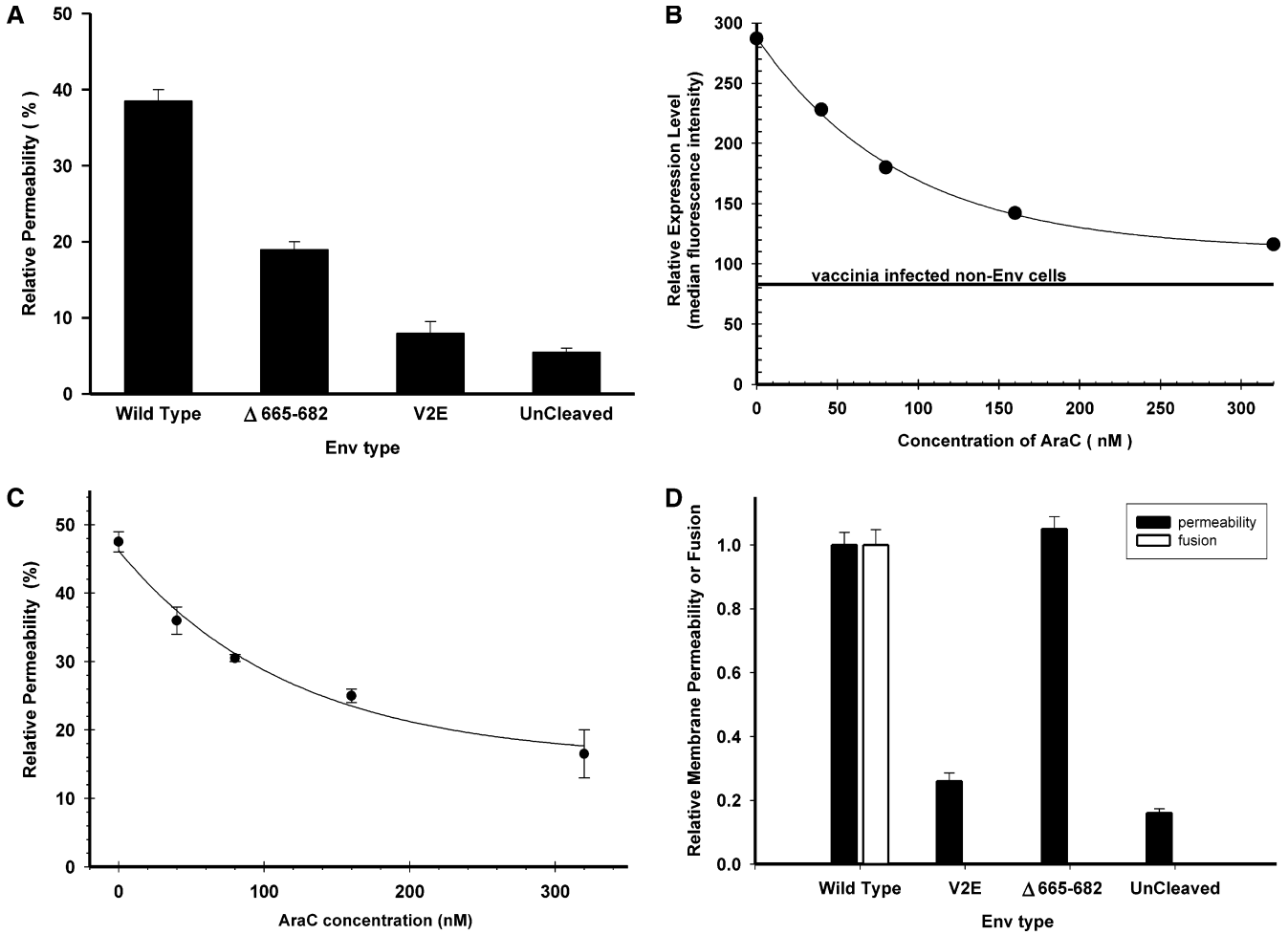

FIGURE 3: (A) Env-expressing HeLa cell membrane permeability changes after incubation for 20 min with bead−CD4−CXCR4 complexes at 37 °C. The values are as follows: 38.0 ± 2.0% for the wild-type Env, 19.0 ± 1.0% for Δ665−682 Env, 8.5 ± 1.5% for V2E Env, and 5.5 ± 0.5% for the uncleaved Env. (B) Expression of the wild-type Env, measured by the median fluorescence intensity, as a function of AraC (cytosine β-D-arabinofuranoside) concentration. The solid line shows the median fluorescence intensity value of the non-Env-expressing cells, i.e., vTF7.3-infected HeLa cells. (C) Permeability of wild-type Env-expressing cells as a function of AraC (cytosine β-D-arabinofuranoside) concentration. (D) Permeability of the Env-expressing cells (black bars) normalized with the permeability of the wild-type Env-expressing cells that have the same Env expression level as the respective mutant Env. The white bar represents cell−cell fusion.

surface. Figure 4 shows only a part of each image. Full-sized images are available in the Supporting Information. The relative amounts of detected 6HBs per cell from the full-sized images were as follows: 0.47 ± 0.08 for the wild-type Env, 0.35 ± 0.04 for the V2E Env, 0.23 ± 0.03 for the Δ665−682 Env, and 0.12 ± 0.02 for the uncleaved Env. Figure 4B shows the relative amounts of the 6HBs on the mutant Env cell surface in comparison to the amount of wild-type Env after normalization with the Env expression level. In comparison to the bead−CD4−CXCR4 complexes, the conformational changes induced by the target cells were quite few in number to be statistically distinguished from the background staining. Images of 6HB occurrences in the Env-expressing target cell contact are available from the authors.

DISCUSSION

The essential role of the viral fusion protein is to accelerate the rate of fusion, i.e., lower the activation energy for fusion. The resolution of the gp41 core structure (*31*−*34*) has led to the notion that six-helix bundle formation drives the target membrane into the proximity of the viral membrane. However, this is not sufficient to induce fusion. In addition, the destabilization of the lipid bilayer as a result of the interaction of other segments of fusion proteins with membranes appears to be needed to lower these barriers (*11*, *12*).

Many studies have been carried out on the interactions of synthetic peptides mimicking the N-terminal fusion peptide region of gp41 (*35*) with lipid bilayers. Synthetic fusion peptides, which promote liposome fusion, are capable of destabilizing membrane bilayers (*36*). One motif for destabilizing membranes that appears to be common to a number of diverse fusion systems is for the entry of the peptide into the membrane as an α-helix inserted at an oblique angle (*37*). This motif has been demonstrated by polarized Fourier transform infrared spectroscopy (FTIR) on viral fusion peptides and has been shown to correlate with the fusogenic activity of the intact virus (*38*). It should be pointed out, however, that modeling the membrane-inserted fusion peptide as a rigid α-helix is likely to be an oversimplification. Tamm and co-workers showed that the fusion peptide of influenza virus inserts into a membrane in a distorted helix with a kinked structure (*39*). A combination of ^{13}C-enhanced FTIR with molecular simulations has been used to study the secondary conformation of the synthetic HIV-1 gp41 fusion peptide in aqueous, structure-promoting, lipid, and biomem-

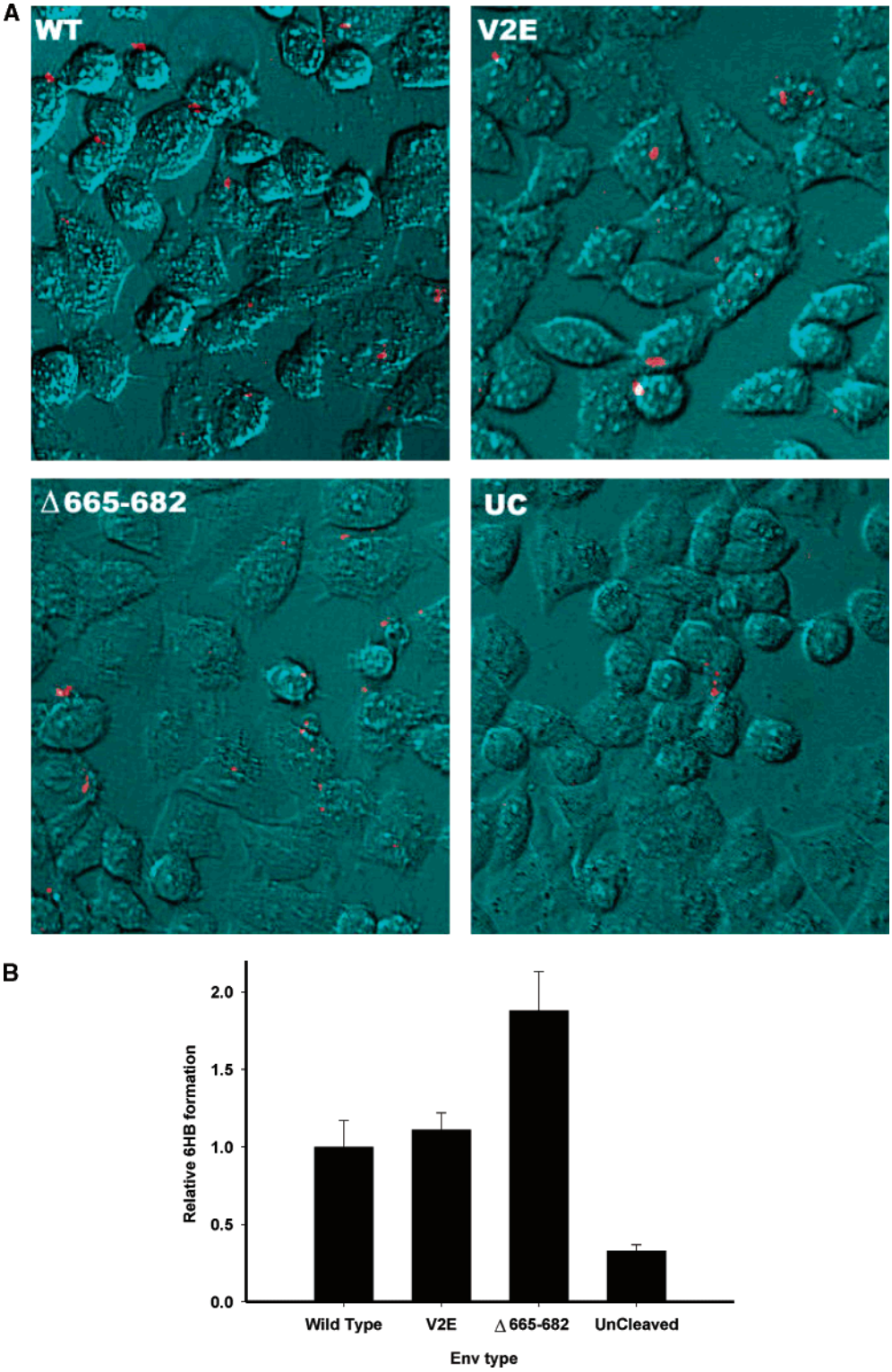

FIGURE 4: Six-helix bundle (6HB) on Env-expressing HeLa cells, visualized by immunostaining with NC-1 mAb and Cy5-conjugated anti-mouse Fab as the secondary antibody. (A). HeLa cells expressing wild-type, V2E, Δ665−682, and uncleaved HIV-1 Env were incubated for 5 min with bead−CD4−CXCR4 complexes. The staining procedure is described in Experimental Procedures. Full-sized images are available in the Supporting Information. Each full-sized image contains between 300 and 500 individual cells and represents an overlay of a differential interferometry contrast (DIC) image and a fluorescence image. The view in DIC is shown in a blue-green color. The spotted red dots show the positions of the 6HB mapped by NC-1 mAb and Cy5-conjugated goat anti-mouse Fab. The fluorescent image overlays were optimized to keep intensities between 260 and 1024, where only the positive signal from 6HB staining remains visible. (B). Relative amounts of NC-1-stained 6HBs per cell: 0.47 ± 0.08 for the wild-type Env, 0.35 ± 0.04 for the V2E Env, 0.23 ± 0.03 for the Δ665−682 Env, and 0.12 ± 0.02 for the uncleaved Env. The bars were calculated according to the equation O = dens/(0.47 × exrs), where dens is the relative amount of NC-1-stained 6HBs per cell and exrs is the relative level of Env expression assuming wild-type Env expression for 1.00. The values of exrs, calculated from the data in Figure 1, are 1.00 for the wild-type Env, 0.67 for the V2E Env, 0.26 for the Δ665−682 Env, and 0.81 for the uncleaved Env. The normalization factor of 0.47 is the average relative density of 6HB on the WT Env-expressing cells. The apparent enhancement of the relative formation of the Δ665−682 6HBs is most probably due to the inclusion of the background signal, which has been normalized by an exrs of 0.26 as stated above.

brane environments (*40*). These studies indicate that at low peptide loading levels in human erythrocyte ghost membranes the central core of the fusion peptide (residues 5−15) assumed α-helical conformations. On the other hand, at high peptide loading levels, the central core of the fusion peptide assumed an antiparallel *β*-structure (*41*). It is tempting to speculate that the α-helical conformations at low peptide loading levels are associated with fusion and that the *β*-structures at high peptide loading levels are associated with membrane permeabilization. This is consistent with the observations by Haque and Lentz (*42*) that at low peptide: lipid ratios (<1:200) the gp41 fusion peptide enhances polyethylene glycol-mediated fusion of highly curved small unilamellar vesicles, whereas at higher peptide:lipid ratios, the peptide induces rupture of the vesicles. The insertion of the peptide into the outer monolayer of the membrane presumably results in a rapid expansion of the area of the outer monolayer (*43*, *44*). The bending stress of the outer monolayer may be relieved by rapid flip-flop of phospholipid (*45*) and peptide from the outer to inner monolayer followed by the formation of nanometer-scale pores.

The fusion peptide is not the only peptide from the gp41 sequence which can induce liposome−lipid mixing and destabilization. The peptide mimicking the membrane-proximal domain has been shown to induce lipid mixing and destabilization of liposomes with an efficiency even higher than that of the fusion peptide, suggesting that this peptide may play a similar role in the intact envelope glycoprotein (*21*).

In this study, we have focused on the roles of the N-terminal fusion peptide and the membrane-proximal sequences of the intact HIV-1 gp41 in the setting of a biological fusion reaction. We had previously developed an assay for membrane destabilization monitored by the influx of Sytox, an impermeant fluorescent dye, into the Env-expressing cells following the interaction with CD4−CXCR4 complexes (*7*). We monitored fusion by observing dye transfer between Env-expressing cells and appropriate target cells, a well-established methodology in our laboratory (*46*). We then examined how mutations in these two regions might affect the fusion and destabilization phenotypes. As expected from previous studies (*19*, *22*), both fusion peptide and membrane-proximal mutants did not promote fusion (Figure 2).

Env expression on the cell surface affects the fusion progress (*28*). Our data (see Figure 3) show that Env expression also plays a significant role in the permeabilization of the cell membranes. The level of wild-type Env surface expression in our experiments was slightly higher than the level of V2E and uncleaved Env surface expression. The level of surface expression of Δ665−682 Env was ∼4 times lower than the level of surface expression of wild-type Env (Figure 1). However, after the level of wild-type Env expression had been reduced to that of the mutant with a deleted region, Δ665−682, both Envs exhibited the same ability to permeabilize their own membrane. This indicates that the membrane-proximal domain does not affect the ability of the gp41 to induce membrane permeabilization. On the other hand, the V2E mutant induced little permeabilization over background (Figure 3), which confirms the primary role of the fusion peptide in the membrane permeabilization process.

To rule out the possibility that a failure of the mutant Envs to induce fusion and/or permeabilization was due a triggering defect, we examined Env conformational changes following their interactions with CD4 and CXCR4 by immunofluorescence. We used the anti-gp41 mAb NC-1 that reacts with the six-helix bundle (*27*) (Figure 4). To properly quantify the occurrences of 6HB formation, we used bead−CD4−CXCR4 complexes. The large amount of active CD4 and CXCR4, which was released by the protein G beads, triggered massive conformational changes. Figure 4B shows the relative amount of 6HBs formed on each Env-expressing cell membrane upon interaction with CD4 and CXCR4. The 6HB densities on the wild-type Env-, V2E Env-, and Δ665−682 Env-expressing cell surfaces were significantly higher than on the control uncleaved Env-expressing cell surface. These results indicate that the mutant Envs, V2E and Δ665−682, are triggered even in the absence of fusion.

Current models of HIV-1 Env-mediated fusion posit that the gp41 fusion peptide inserts into the target membrane in the prehairpin state (*8*). These models are supported by the observation that target cells expressing membrane-anchored T20 (DP178) are not susceptible to infection by HIV-1 virions (*47*). This indicates that the fusion peptide must be inserted into the target membrane for antiparallel binding of the T20 to the N-terminal grooves to occur. If fusion could occur solely via self-insertion, which presumably would create a prehairpin structure to form perpendicular to the membrane, only parallel binding of T20 would be allowed and, therefore, fusion would be rendered insensitive to inhibition, which is clearly not the case. Similar data on SIV Env-mediated fusion were obtained using fatty acyl-linked SIV gp41-derived T20 (*48*). The evidence favors "pull" models that couple the energy of coil−coil formation to the movement of the target membrane toward the viral membrane rather than "push" models that couple this energy to the bulging of viral membranes as a result of fusion peptide self-insertion (*49*).

The membrane permeabilization observed when Env-expressing cells are challenged with an abundance of CD4 and coreceptor complexes either attached to beads or on cells would then be due to the inactivation that leads to self-insertion of fusion peptides. Such self-insertion as a result of inactivation has been observed in the case of influenza hemagglutinin (*50*, *51*).

The roles of the fusion peptide and membrane-proximal region are summarized in the simplified model shown in Figure 5. Following the triggering of Env by CD4 and coreceptor, the gp41 is free to swing out, insert into the target membrane, and bring the two membranes together, resulting in fusion (top left panel). Under conditions of inactivation, in the absence of the target, it swings back into its own membrane, resulting in membrane permeabilization (bottom left panel). The mutant, V2E Env, which is free to expose its gp41 fusion peptide, cannot insert into the cell membrane and facilitate the fusion process (top middle panel), nor can it insert back into its own membrane following inactivation (bottom middle panel). Our observation that V2E does not permeabilize the membrane despite an intact membrane-proximal region indicates that the latter domain is not responsible for destabilization of the biological membranes. However, this region is crucial for membrane fusion. Our data are consistent with the notion that in the absence of the

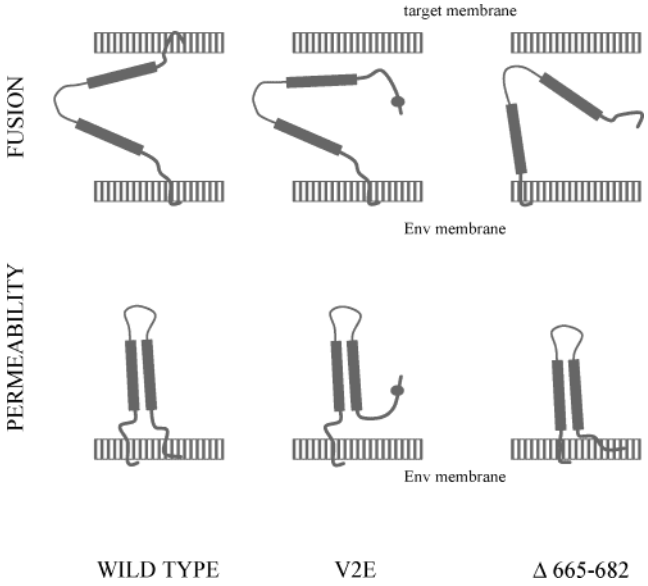

FIGURE 5: Schematics of hypothetical intermediates that are critical for the membrane fusion or membrane destabilization by CD4 and CXCR4. The wild-type Env gp41 has an unmodified fusion peptide and ectodomain. Fusion proceeds in the presence of the target membrane. The membrane permeabilization occurs in an excess of CD4 and coreceptor molecules. The V2E Env has nonfunctional fusion peptide, which cannot insert into the plasma membrane. Because of this inability, we observed neither fusion nor permeabilization. The mutant gp41 Env with residues 665−682 deleted most probably became too stiff due to the shortened distance between the membrane and the C-terminal helices. Mechanistically, the developed stiffness does not allow free bending of gp41 to reach the target membrane and initiate fusion. The Env-expressing membrane, however, is easily accessible, and the membrane destabilization proceeds as well as with the wild-type Env.

supporting 18-amino acid region the exposed fusion peptide might be unable to bend back, reach the target membrane, and bring it close to the Env membrane (top right panel). However, under conditions of inactivation, the exposed fusion peptide is still capable of self-insertion as evidenced by the increase in membrane permeability (bottom right panel).

In conclusion, we have studied the phenotypes of gp41 mutants in the two regions that are crucial to fusion using two different assays. In conjunction with conformationally sensitive antibodies, our study gives a more refined and complete picture of the pathway to the membrane fusion, i.e., from the interaction of Env with CD4 and CXCR4 to the formation of the fusion pore. The membrane permeability studies may have bearing upon cell killing. According to a model proposed by Sodroski and co-workers (*52*), infection of cells by HIV-1 would involve expression of Env in the membranes of the Golgi apparatus. The encounter of Env with CD4 and coreceptor in the Golgi would then lead to the insertion of fusion peptide and the creation of numerous pores. As membrane damage exceeds the repair capacity of the cell, death ensues.

ACKNOWLEDGMENT

The following reagents were obtained through the AIDS Research and Reference Reagent Program, Division of AIDS, NIAID, NIH: U373-MAGI-CXCR4 cells were from Dr. Michael Emerman. We are grateful to Dr. Edward Berger and Dr. Karl Salzwedel for supplying the plasmids and Dr. Christopher Broder for the T8 antibody. We thank our colleagues Anu Puri, Dimiter Dimitrov, Julie Eaton, Mathias Viard, Sanjay Phogat, Steve Gallo, Yuuei Shu, Yossef Raviv, and Xiaodong Xiao for the fruitful discussions and continuous help during this study. We thank the Fellow Editorial Board at the National Cancer Institute, Center for Cancer Research, for the critical review and useful suggestion on the presentation style.

SUPPORTING INFORMATION AVAILABLE

Four images showing occurrences of the 6HB on HeLa cells expressing wild-type, V2E, Δ665−682, and uncleaved HIV-1 Env after incubation for 5 min with bead−CD4−CXCR4 complexes (portions of these full-sized images shown in Figure 4A). This material is available free of charge via the Internet at http://pubs.acs.org.

REFERENCES

1. Berger, E. A. (1997) *AIDS 11* (Suppl. A), S3−S16.
2. Doms, R. W., and Peiper, S. C. (1997) *Virology 235*, 179−190.
3. Moore, J. P., Trkola, A., and Dragic, T. (1997) *Curr. Opin. Immunol. 9*, 551−562.
4. Salzwedel, K., Smith, E. D., Dey, B., and Berger, E. A. (2000) *J. Virol. 74*, 326−333.
5. Jones, P. L., Korte, T., and Blumenthal, R. (1998) *J. Biol. Chem. 273*, 404−409.
6. Dimitrov, D. S. (2000) *Cell 101*, 697−702.
7. Dimitrov, A. S., Xiao, X., Dimitrov, D. S., and Blumenthal, R. (2001) *J. Biol. Chem. 276*, 30335−30341.
8. Chan, D. C., and Kim, P. S. (1998) *Cell 93*, 681−684.
9. Sodroski, J. G. (1999) *Cell 99*, 243−246.
10. Moore, J. P., and Stevenson, M. (2000) *Nat. Rev. Mol. Cell Biol. 1*, 40−49.
11. Blumenthal, R., Clague, M. J., Durell, S. R., and Epand, R. M. (2003) *Chem. Rev. 103*, 53−69.
12. Gallo, S. A., Finnegan, C. M., Viard, M., Raviv, Y., Dimitrov, A., Rawat, S. S., Puri, A., Durell, S., and Blumenthal, R. (2003) *Biochim. Biophys. Acta 1614*, 36−50.
13. Jiang, S., Lin, K., Strick, N., and Neurath, A. R. (1993) *Nature 365*, 113.
14. Kliger, Y., Gallo, S. A., Peisajovich, S. G., Munoz-Barroso, I., Avkin, S., Blumenthal, R., and Shai, Y. (2001) *J. Biol. Chem. 276*, 1391−1397.
15. Gallo, S. A., Puri, A., and Blumenthal, R. (2001) *Biochemistry 40*, 12231−12236.
16. Chan, D. C., Chutkowski, C. T., and Kim, P. S. (1998) *Proc. Natl. Acad. Sci. U.S.A. 95*, 15613−15617.
17. Furuta, R. A., Wild, C. T., Weng, Y., and Weiss, C. D. (1998) *Nat. Struct. Biol. 5*, 276−279.
18. Wild, C. T., Shugars, D. C., Greenwell, T. K., McDanal, C. B., and Matthews, T. J. (1994) *Proc. Natl. Acad. Sci. U.S.A. 91*, 9770−9774.
19. Salzwedel, K., West, J. T., and Hunter, E. (1999) *J. Virol. 73*, 2469−2480.
20. Munoz-Barroso, I., Salzwedel, K., Hunter, E., and Blumenthal, R. (1999) *J. Virol. 73*, 6089−6092.
21. Suarez, T., Gallaher, W. R., Agirre, A., Goni, F. M., and Nieva, J. L. (2000) *J. Virol. 74*, 8038−8047.
22. Freed, E. O., Myers, D. J., and Risser, R. (1990) *Proc. Natl. Acad. Sci. U.S.A. 87*, 4650−4654.
23. Kliger, Y., Aharoni, A., Rapaport, D., Jones, P., Blumenthal, R., and Shai, Y. (1997) *J. Biol. Chem. 272*, 13496−13505.
24. Elson, H. F., Dimitrov, D. S., and Blumenthal, R. (1994) *Mol. Membr. Biol. 11*, 165−169.
25. Broder, C. C., and Berger, E. A. (1995) *Proc. Natl. Acad. Sci. U.S.A. 92*, 9004−9008.
26. Earl, P. L., Koenig, S., and Moss, B. (1991) *J. Virol. 65*, 31−41.
27. Jiang, S., Lin, K., and Lu, M. (1998) *J. Virol. 72*, 10213−10217.

28. Lineberger, J. E., Danzeisen, R., Hazuda, D. J., Simon, A. J., and Miller, M. D. (2002) *J. Virol. 76*, 3522−3533.
29. Xiao, X., Wu, L., Stantchev, T. S., Feng, Y. R., Ugolini, S., Chen, H., Shen, Z., Riley, J. L., Broder, C. C., Sattentau, Q. J., and Dimitrov, D. S. (1999) *Proc. Natl. Acad. Sci. U.S.A. 96*, 7496−7501.
30. Finnegan, C. M., Berg, W., Lewis, G. K., and Devico, A. L. (2002) *J. Virol. 76*, 12123−12134.
31. Weissenhorn, W., Dessen, A., Harrison, S. C., Skehel, J. J., and Wiley, D. C. (1997) *Nature 387*, 426−430.
32. Chan, D. C., Fass, D., Berger, J. M., and Kim, P. S. (1997) *Cell 89*, 263−273.
33. Tan, K., Liu, J., Wang, J., Shen, S., and Lu, M. (1997) *Proc. Natl. Acad. Sci. U.S.A. 94*, 12303−12308.
34. Caffrey, M., Cai, M., Kaufman, J., Stahl, S. J., Wingfield, P. T., Covell, D. G., Gronenborn, A. M., and Clore, G. M. (1998) *EMBO J. 17*, 4572−4584.
35. Durell, S. R., Martin, I., Ruysschaert, J. M., Shai, Y., and Blumenthal, R. (1997) *Mol. Membr. Biol. 14*, 97−112.
36. Epand, R. M. (1998) *Biochim. Biophys. Acta 1376*, 353−368.
37. Brasseur, R. (1991) *J. Biol. Chem. 266*, 16120−16127.
38. Horth, M., Lambrecht, B., Khim, M. C., Bex, F., Thiriart, C., Ruysschaert, J. M., Burny, A., and Brasseur, R. (1991) *EMBO J. 10*, 2747−2755.
39. Han, X., Bushweller, J. H., Cafiso, D. S., and Tamm, L. K. (2001) *Nat. Struct. Biol. 8*, 715−720.
40. Gordon, L. M., Mobley, P. W., Pilpa, R., Sherman, M. A., and Waring, A. J. (2002) *Biochim. Biophys. Acta 1559*, 96−120.
41. Saez-Cirion, A., and Nieva, J. L. (2002) *Biochim. Biophys. Acta 1564*, 57−65.
42. Haque, M. E., and Lentz, B. R. (2002) *Biochemistry 41*, 10866−10876.
43. Blumenthal, R., and Morris, S. J. (1999) *Mol. Membr. Biol. 16*, 43−47.
44. Longo, M. L., Waring, A. J., and Hammer, D. A. (1997) *Biophys. J. 73*, 1430−1439.
45. Raphael, R. M., and Waugh, R. E. (1996) *Biophys. J. 71*, 1374−1388.
46. Blumenthal, R., Gallo, S. A., Viard, M., Raviv, Y., and Puri, A. (2002) *Chem. Phys. Lipids 116*, 39−55.
47. Hildinger, M., Dittmar, M. T., Schult-Dietrich, P., Fehse, B., Schnierle, B. S., Thaler, S., Stiegler, G., Welker, R., and von Laer, D. (2001) *J. Virol. 75*, 3038−3042.
48. Peisajovich, S. G., Gallo, S. A., Blumenthal, R., and Shai, Y. (2003) *J. Biol. Chem. 278*, 21012−21017.
49. Kozlov, M. M., and Chernomordik, L. V. (1998) *Biophys. J. 75*, 1384−1396.
50. Weber, T., Paesold, G., Galli, C., Mischler, R., Semenza, G., and Brunner, J. (1994) *J. Biol. Chem. 269*, 18353−18358.
51. Wharton, S. A., Calder, L. J., Ruigrok, R. W., Skehel, J. J., Steinhauer, D. A., and Wiley, D. C. (1995) *EMBO J. 14*, 240−246.
52. LaBonte, J. A., Madani, N., and Sodroski, J. (2003) *J. Virol. 77*, 6645−6659.

BI035154G